Available online at www.sciencedirect.com
SCIENCE DIRECT®
Polymer 44 (2003) 3363–3373
polymer
www.elsevier.com/locate/polymer

Spatial distribution of molecular orientation in injection molded iPP: influence of processing conditions

R. Mendoza[a], G. Régnier[a,*], W. Seiler[b], J.L. Lebrun[c]

[a]*Laboratoire de Transformation et Vieillissement des Polymères (LTVP)—ENSAM, 151 bd de l'Hôpital 75013, Paris, France*
[b]*Laboratoire de Microstructure et Mécanique des Matériaux (LM3-UM12 8006)—ENSAM, 151 bd de l'Hôpital 75013, Paris, France*
[c]*Laboratoire des Procédés, Matériaux et Instrumentation (LPMI)—ENSAM, 2 bd du Ronceray 49035, Angers, France*

Received 14 November 2002; received in revised form 21 March 2003; accepted 21 March 2003

Abstract

In this paper, the influence of processing conditions on the spatial distribution of the molecular orientation was determined within the depth of the thickness of injection molded isotactic polypropylene (iPP) plates. Small 35 μm-thick slices were microtomed from the surface to the core of 1 and 3 mm-thick plates. The orientation functions along the three crystallographic axes were determined on the slices from IR dichroism measurements and WAXS pole figures. It was found that the orientation of the amorphous phase was low and the crystalline orientation had a maximum in the shearing layer, which was solidified during the filling stage. The plate thickness seemed to govern the global level of orientation, while the injection speed determined the thickness of the shearing layer without changing the maximum of orientation. Changing the mold temperature from 20 to 40 °C did not modify the molecular orientation. A specific bimodal crystalline orientation was found in the shearing layer. This crystalline structure continued in the post-filling layer, but the local symmetry axes tilted towards the core.

Keywords: Injection molding; Molecular orientation; Isotactic polypropylene

1. Introduction

Injection molding is a widely extended process characterized by high production rates and tight geometrical tolerances. Simulations of the filling phase are usually performed to optimize the feeding system and the gate geometry, the weld-lines, the thickness of the part or the filling flux equilibrium. To reduce further the high tool costs, and limit the mold modifications, in-plane shrinkages and warpage predictions are required, but the thermo-mechanical calculation, including the modeling of solidification, which should be performed is very complex. Data on the mechanical properties of the material are needed, especially on the moduli and the thermal expansion coefficients. As the mold shrinkages are anisotropic [1], anisotropic mechanical properties, which depend on the molecular orientation [2], have to be determined.

The molecular orientation, which is frozen in the solid polymer, is induced by a very complex flow during the three stages of the process: the mold filling, the post-filling, which compensates the thermal shrinkage, and the additional cooling to solidify the center of the part [3]. Basically, it has been suggested that the molecular orientation in the flow direction at the skin layer is due to the fountain like flow, which generates an extensional flow [4]. Towards the center of the part, the shear flow has a dominant influence on the molecular orientation, orienting the molecules mainly in the flow direction. Molding conditions, such as melt temperature, mold temperature or injection speed, could affect the level of molecular orientation [5].

Here, we must distinguish between amorphous and semi-crystalline polymers. For injection molded amorphous polymers, the molecular orientation is due to the non-relaxed orientation generated by the melt flow. This frozen molecular orientation can be easily determined by birefringence [5,6] and predicted by considering the viscoelastic behavior of the polymer melt [7]. Whatever the processing conditions, the molecular orientation leads to small in-plane shrinkages and quasi-isotropic mechanical properties [8].

* Corresponding author. Tel.: +33-144-246-305; fax: +33-144-246-382.
E-mail address: gilles.regnier@paris.ensam.fr (G. Régnier).

0032-3861/03/$ - see front matter © 2003 Elsevier Science Ltd. All rights reserved.
doi:10.1016/S0032-3861(03)00253-2

For semi-crystalline polymers, the molecular orientation in the melt which is being cooled generates an oriented crystallization and therefore, the global orientation in the solid polymer is generally higher than the one which existed in the sheared melt [9]. Unlike amorphous polymers, high anisotropy of in-plane shrinkage and mechanical properties could be obtained in injected semi-crystalline polymers [1].

Although the structural development in injection molded isotactic polypropylene (iPP) has been widely studied [10,11,12], the aim of this paper is to show the influence of processing conditions and especially the influence of the thickness of the part on the spatial distribution of the molecular orientation within the depth from infrared dichroism and WAXS measurements.

2. Experimental procedures

2.1. Material and injection conditions

A commercial homopolymer polypropylene ELTEX PP HV 252 from Solvay was chosen for the study (MFI = 11 g/min for 2.16 kg at 230 °C). The molecular weight (M_w = 180.8 g/mol), and the polydispersity index (M_w/M_n = 7.3) were measured by Solvay by means of gel permeation chromatography.

The mold cavity is a square slab of 60 × 60 mm^2, gated through an end fan-gate with a thickness of 0.8 mm for the 1 mm-thick plate, and 1.5 mm for the 3 mm-thick plate (Fig. 1). These mold cavities have a specific fish tail feeding system in order to obtain a polymer front parallel to the gate [13].

The material was injected in a DK CODIM 175-400 injection press with a barrel diameter of 36 mm. The melt temperature was set to 220 °C, the hold pressure at the nozzle to 40 MPa, the holding time to 5 s for the 1 mm-thick plate and 12 s for the 3 mm-thick plate, and the total cooling time to 15 and 40 s, respectively. It was checked that the gates were frozen before the end of the holding time.

Two processing parameters were varied in the study: the mold temperature and the injection speed. The mold temperature was varied from 20 to 40 °C. Two injection speeds were set in order to obtain the same polymer front velocity for both thickness by measuring a lapse of time of 0.1 and 0.3 s between the two pressure sensor records spaced 30 mm apart in the mold cavity (Fig. 1). This gave two respective injection times of 0.7 and 1.6 s approximately.

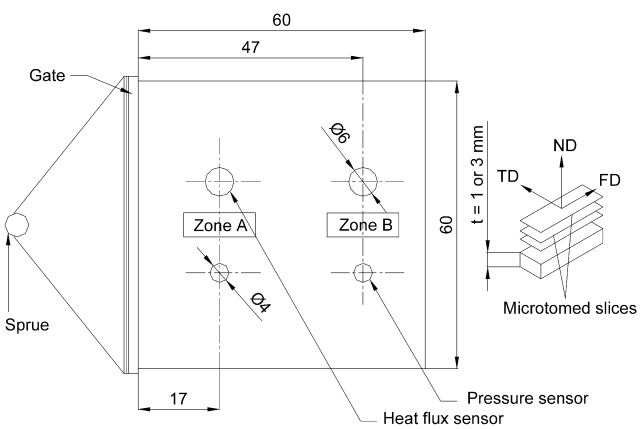

Fig. 1. Geometry of the injected plate, localization of the sensors and of the measured zones and definition of the specimen reference axes.

2.2. Sample preparation

The studied zones were located 17 mm (zone A) and 47 mm (zone B) from the gate, close to the center of the part (Fig. 1). Samples of 5 mm × 15 mm were cut from the molded plates. Slices of 35 μm were cut parallel to the flow direction (FD) in the FD–transverse direction (TD) plane using a Reichert-Jung Mod 1140 Autocut microtome.

Although the microtoming technique is open to criticism [14], and even if Excimer laser layer removal should be preferred [15], it was possible to optimize the cutting parameters (cutting speed, and cutting angle) in order to minimize the influence of microtoming on the molecular orientation measurement, according to Lundberg et al. [16]. The same samples were microtomed in two orthogonal directions (transverse and flow directions) and the molecular orientation was measured by infrared dichroism. Cutting conditions were chosen to give a difference between the two orthogonally cut slices of less than 0.02 in terms of Herman's orientation function (see below): cutting speed = 100 mm/s, cutting rake angle = 36° at ambient temperature.

The recent microbeam WAXS method could be a good alternative to the microtoming technique for investigating the sharp structural gradients of molecular orientation that are observed in injection molded parts [17], but requires large experimental resources (synchrotron radiation).

2.3. Infrared dichroism measurements

Infrared dichroism measurements are rapid and quite easy to perform although a lot of care has to be taken when performing the base line determination [18]. Biaxial orientations in films can be determined with the 'tilted film' technique [19,20]. Nevertheless, in order to quickly obtain orientation measurements within the depth for the different processing conditions, we assumed that the molecular chain spatial distribution has a cylindrical symmetry in the flow direction axis, as several researchers have recently done [21,22]. Therefore, to quantify the chain orientation in the flow direction, the second order Hermans-type orientation function was calculated by taking the flow direction as reference axis [23]

$$f = \frac{3\langle\cos^2\phi\rangle - 1}{2} = \left(\frac{D-1}{D+2}\right)\left(\frac{2\,\mathrm{cotan}^2\alpha + 2}{2\,\mathrm{cotan}^2\alpha - 1}\right) \quad (1)$$

where ϕ is the angle between the chain axis and the flow direction, D is the dichroic ratio and α the transition-moment dipole angle. For the molecular orientation function, a value of zero represents an isotropic polymer, a value of one a perfectly aligned polymer along the reference axis, and a value of -0.5 a perfect orientation which is normal with respect to the reference axis. The cylindrical symmetry of the structure around the flow direction will be discussed later in the paper and the crystalline phase orientation function determined from infrared dichroism measurements will be compared to the chain orientation function in the flow direction f_{cF} determined by WAXS pole figures.

The molecular orientation was determined in the A and B zones (Fig. 1) using an infrared spectrometer Bruker IFS-28. The 998 cm^{-1} peak with a transition-moment angle of 18° was used to determine the crystalline phase orientation function, the 1256 cm^{-1} peak with a transition-moment angle of 0° for the average orientation function, and the 2725 cm^{-1} peak with a transition-moment angle of 90° for the amorphous phase orientation function [24].

2.4. WAXS measurements

WAXS measurements were performed in a Philips X'pert MRD diffractometer employing punctual Cu Kα radiation at 40 mA and 40 kV on the same slices as the ones used for infrared dichroism measurements. Since our specimens have a very low volume ($5 \times 15 \times 0.035$ mm^3) and our X-ray diffractometer has a small power, the beam dimensions has to be widened as much as possible to do the measurements in a reasonable time. As the sample area is small, if a wide beam and a conventional diffraction technique is used, the beam will be wider than the sample as the azimuthal angle is increased, and the measurement will be not valid. To solve this problem a constant area technique was used in such a way that all the available matter volume interacted with the X-rays during the whole measurement. In the transmission mode, a steel sheet of 0.18 mm with a 3 mm-diameter hole was placed between the specimen and the beam. Therefore, the specimen area, which interacts with the beam, is always constant whatever the azimuthal angle. The hole size was chosen to allow easy sample positioning. In the reflection mode, a 4 mm-round specimen was stuck on an aluminum plate using an amorphous resin. The primary X-ray beam had a low divergence (parallel beam optic).

DSC measurements showed that the microtomed specimens in the shearing and post-filling layers (see below) could exhibit some β phase traces, except for the shearing layer of the 3 mm-thick plate, β phase ratio reaching 4 or 5%. Then, it was decided to study only the molecular orientation of the α phase. The spatial distribution of the diffracted intensity of Bragg's family planes (110) and (040) for the α phase of iPP was recorded at a 2θ angle of 14.1 and 16.9°, respectively.

The diffracted intensity was measured in the transmission mode and in the reflection mode since neither of the two modes covers all the space by itself. The spatial distribution of the diffracted intensity was obtained by a two angles scanning: the scans in the transmission mode were made with the χ_{trans} angle ranging from -90 to 90° and ϕ_{trans} from -70 to 70°, for the reflection mode the scans were made with χ_{reflex} ranging from 0 to 70° and ϕ_{reflex} from 0 to 360° (Fig. 2). Angular steps of 5° were performed for ϕ and χ for both diffraction modes. Pole figures were plotted according to a meridional stereographic representation (Wulff representation) [25].

The crystalline diffracted intensity values were corrected for background, absorption and defocalization effects. The background was measured by means of θ–2θ scans in every ϕ_{trans} position for the transmission mode, and in every χ_{reflex} position for the reflexion mode. The absorption and defocalization corrections were made using a non-oriented specimen of the same thickness [25]. The corrected intensity values obtained in the reflection mode were adjusted to the same intensity level as the transmission ones using the common points of measurement. The small zones of the space that were not reached by the scans in the transmission and reflection modes were interpolated (Fig. 2).

From the intensities measured, the $\langle \cos^2 \phi_{hkl,J} \rangle$ could be calculated using the following expressions [26]

$$\langle \cos^2 \phi_{hkl,F} \rangle = \frac{\int_0^{2\pi} \int_0^{\pi/2} I(\phi,\beta) \cos^2\phi \sin\phi \, d\phi \, d\beta}{\int_0^{2\pi} \int_0^{\pi/2} I(\phi,\beta) \sin\phi \, d\phi \, d\beta} \quad (2a)$$

$$\langle \cos^2 \phi_{hkl,T} \rangle = \frac{\int_0^{2\pi} \int_0^{\pi/2} I(\phi,\beta) \sin^3\phi \cos^2\beta \, d\phi \, d\beta}{\int_0^{2\pi} \int_0^{\pi/2} I(\phi,\beta) \sin\phi \, d\phi \, d\beta} \quad (2b)$$

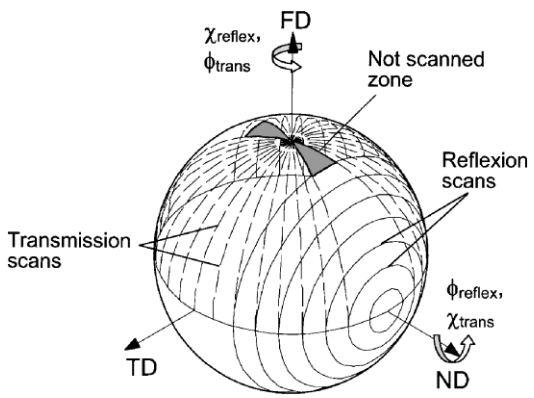

Fig. 2. Path of the scans and angle definitions in WAXS transmission and reflexion modes.

$$\langle \cos^2 \phi_{hkl,N} \rangle = \frac{\int_0^{2\pi} \int_0^{\pi/2} I(\phi,\beta) \sin^3 \phi \sin^2 \beta \, d\phi \, d\beta}{\int_0^{2\pi} \int_0^{\pi/2} I(\phi,\beta) \sin \phi \, d\phi \, d\beta} \quad (2c)$$

where $\phi_{hkl,J}$ is the angle between the normal of the (hkl) plane and the J direction (flow, transverse or normal direction), β is the azimuthal angle around the J direction. As there are no strong diffractions of (l00) planes (a-crystallographic axis or crystal growth direction) nor of (00l) planes (c-crystallographic axis or chain direction) in the α phase, it is possible to determine the mean-square cosine of ϕ angle from the unit cell geometry and the diffraction intensities from the (110) and (040) planes [27]:

$$\langle \cos^2 \phi_{c,J} \rangle = 1 - 1.099 \langle \cos^2 \phi_{110,J} \rangle - 0.901 \langle \cos^2 \phi_{040,J} \rangle \quad (3a)$$

$$\langle \cos^2 \phi_{a,J} \rangle = 0.974(1 - \langle \cos^2 \phi_{c,J} \rangle) - 0.947 \langle \cos^2 \phi_{040,J} \rangle \quad (3b)$$

Finally, the Hermans-type orientation function can be calculated

$$f_{p,J} = \frac{3\langle \cos^2 \phi_{p,J} \rangle - 1}{2} \quad (4)$$

where p is the crystallographic axis ($p = a$, b or c). The following equations which link the different orientation functions can be deduced

$$f_{p,F} + f_{p,T} + f_{p,N} = 0 \quad (5)$$

$$f_{a^*,J} + f_{b,J} + f_{c,J} = 1 \quad (6)$$

where a^* is the normal direction to the (b–c) crystallographic plane of α phase unit cell. Eq. (6) is valid for orthorhombic crystals, nevertheless it gives a good approximation for the monoclinic cell of iPP α phase as the β angle between a and c axes of the unit cell is 99.3° [28].

3. Results and discussion

3.1. Orientation measurements by infrared dichroism

The consistency between the three measured orientation functions (Fig. 3) was verified by comparing the measured average orientation (f_{av}) and the calculated one ($f_{av\ Calculated}$) according to the following equation

$$f_{av\ Calculated} = V_c f_{cr} + (1 - V_c) f_{am} \quad (7)$$

where V_c is the crystalline volume fraction. V_c was determined for each microtomed specimen from density measurements using a density gradient column and varied between 0.5 and 0.6.

In Figs. 3 and 4, the morphologies within the depth of the molded plates, which were observed, thanks to a microscope under a polarized light, and the Herman's orientation functions are superimposed. Four layers, which are generally observed in the literature, can be easily distinguished.

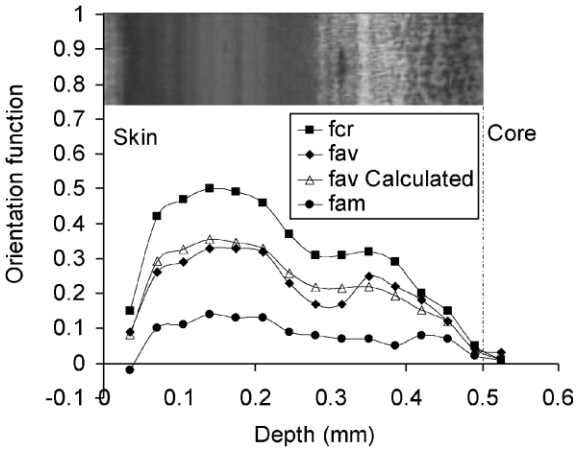

Fig. 3. Molecular orientation functions of the amorphous and the crystalline phases of a 1 mm-thick injected molded iPP plate within the depth. Superimposition of a microscopic view under polarized light. Mold temperature = 40 °C, injection time = 1.6 s, zone A, plate 1.

The first layer at the polymer surface, called the skin layer, is the result of the fast cooling of the molecules which have just been submitted to an extensional deformation in the flow front due to the fountain flow [4]. This layer, which is 30–50 μm thick, seems to have a very high nucleation density because no spherulites are seen. The problems of alignment between the sample and the knife make difficult the obtaining of this layer. A low chain orientation is surprisingly found in this layer.

As the fluid velocity and the shearing stresses are increased, the molecular chains are oriented in the flow direction. The chains, which are close to the solid–liquid boundary, solidify by rapid crystallization preserving the orientation in the flow direction and forming crystallized treads. These treads generally act as nucleus of crystallization of chains that crystallize at lower stress levels. This layer is called the shearing layer and corresponds to the first maximum in the crystalline orientation function (f_{cr}) graph

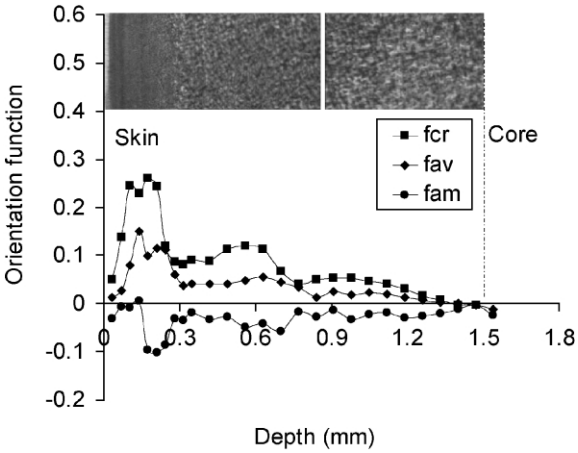

Fig. 4. Molecular orientation functions within the depth of the amorphous and the crystalline phases of a 3 mm-thick injection molded iPP plate. Superimposition of a microscopic view under polarized light. Old temperature = 40 °C, injection time = 1.6 s, zone A, plate 1.

(Figs. 3 and 4). It is 200 μm thick in the samples which were molded at a low injection speed. Very small spherulites could be observed in this layer for the 3 mm-thick plate.

When the mold cavity is full, the flow front stops moving and the shearing stress starts decaying. A minimum in the crystalline orientation function appears, associated with the time delay related to the start of the post-filling stage. After this, a second deformation field is established. Although the shearing stresses in this stage are small, a second maximum of the crystalline orientation function is visible. This layer, called the post-filling layer, is 200 μm-thick for the 1 mm-thick sample and nearly 500 μm-thick for the 3 mm-thick sample. Spherulites are generally observed in this layer, but it is not the case for the 1 mm-thick sample.

Finally when the gate solidifies, the flow stops and the pressure in the mold decreases. The polymer generally crystallizes with a spherulitic morphology. This layer, called the core layer, exhibits a low degree of molecular orientation.

The orientation of the crystalline phase is much greater than the orientation of the amorphous phase, which remains small (less than 0.1). For 3 mm-thick plates, this amorphous orientation remains also small, but negative. A negative orientation of the amorphous phase has already been observed in low-drawn PP films [23]. The molecular orientations of injection molded PS and amorphous PET plates, which were processed with similar processing conditions at the same injection speed, were also measured by infrared dichroism. As very little orientation was found, it can be stated that the large molecular orientation in the injected polymer is given by the orientation of the crystalline phase. As a consequence, the anisotropic material properties of injection molded non-filled semi-crystalline polymers are mainly due to the orientation of the crystalline phase: this partly explains the large shrinkage anisotropy of injected molded parts made of semi-crystalline polymers.

3.1.1. Influence of the thickness

Fig. 5 shows a comparison of the crystalline orientation of the 1 mm-thick plates with that of the 3 mm-thick plates. As the velocity of the polymer front is identical in both cases, a large influence of the cooling (consequently of crystallization kinetics) on the molecular orientation is evident. Injection simulations predict a core layer solidification 2 s after the filling stage for the 1 mm-thick plate and 20 s for the 3 mm-thick plate.

The shearing layer, which is solidified during the filling, is the most oriented zone. The effect of cooling rate variation can be seen by optical microscopy observation of the crystalline microstructure under polarized light: no spherulites are visible for the 1 mm-thick plate, whereas spherulites are even visible in the shearing layer of the 3 mm-thick plates (Figs. 3 and 4).

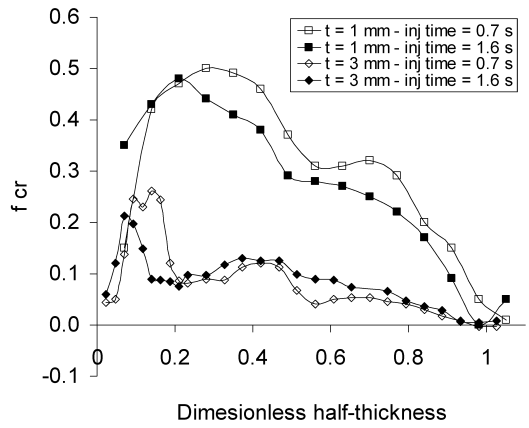

Fig. 5. Influence of the injection time on the molecular orientation functions within the depth of the crystalline phase of a 1 mm and a 3 mm-thick plates. Mold temperature = 40 °C, injection times = 0.7 and 1.6 s, respectively, zone A.

3.1.2. Influence of the injection speed

Tripling the injection speed has paradoxically no large influence compared to tripling of the thickness: the same level of crystalline orientation is reached with the two injection speeds, the first bump is merely narrower and shifted towards the polymer surface (Fig. 6).

3.1.3. Influence of the polymer flow distance

The comparison of the molecular orientation level in the zones A and B shows that the molecular orientation decreases with the polymer flow distance (distance from the gate to the measurement zone) Fig. 7. The thickness of the solidified layer during the mold filling decreases with the flow distance, and although the first maximum, which corresponds to the shearing layer, is narrower, the same level of crystalline orientation is reached. Due to the high polymer viscosity, the pressure loss is large in the plate even during the cooling, therefore the post-filling is less influential when the flow distance increases, which is confirmed by measuring the in-plane shrinkages along the

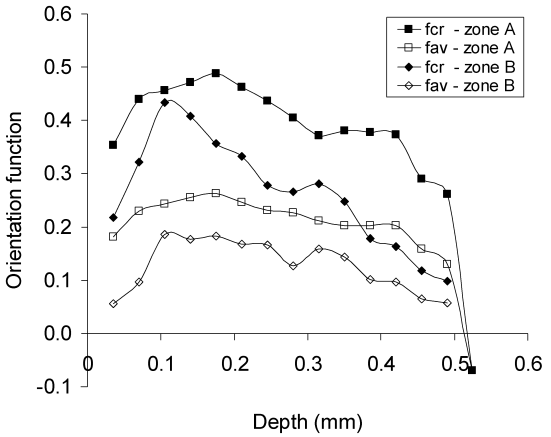

Fig. 6. Influence of flow distance on the molecular orientation function of a 1 mm-thick injection molded iPP plate. Distance between zone A and B = 30 mm, mold temperature = 20 °C, injection time = 1.6 s.

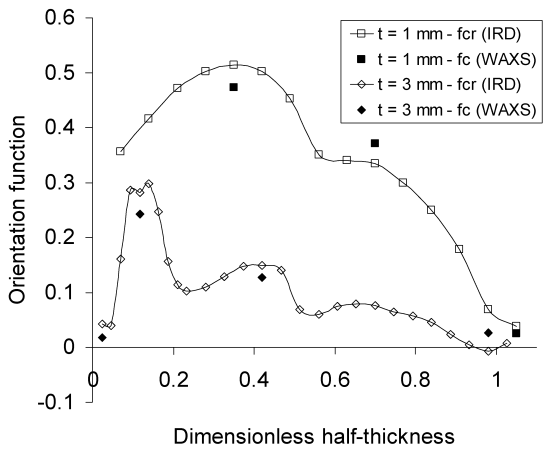

Fig. 7. Comparison of the molecular orientation functions between infrared dichroism and WAXS techniques for a 1 mm and a 3 mm-thick injection molded iPP plates. Mold temperature = 40 °C, injection time = 1.6 s, zone A, plate 2.

flow distance. This fact explains the significant decrease in orientation between the core and the shearing layer when the flow distance is increased.

3.1.4. Influence of the mold temperature

When the mold temperature changed from 20 to 40 °C, there was no evidence of molecular orientation variation, even in the skin. Such a mold temperature variation does not significantly change the polymer cooling rate. It has more influence on the relaxation of the thermal stress, which in turn influences the in-plane shrinkage [1,29], than on molecular orientation.

3.2. WAXS pole figures

The most influential parameter on the molecular orientation level is the thickness of the molded parts, as it can be concluded from the IR dichroism measurements. Therefore, knowing that WAXS measurements require an large amount of experimental work, a comparison between some layers of 1 and 3 mm-thick plates was only performed in the zone A for one process condition: mold temperature = 40 °C and injection time = 1.6 s.

The studied layers to be studied were selected on the basis of the crystalline molecular orientation measurements, which were obtained by IR dichroism (Figs. 3 and 4). The zone A was chosen because it is more discriminant in terms of molecular orientation than the zone B: the solidified layer during the cavity filling is thicker and the effect of post-filling is greater. The microtomed specimens studied in the shearing and post-filling layers were chosen at the locations where the crystalline molecular orientation was maximum. Microtomed specimens in the core and in the skin for the 3 mm-thick plate were also analyzed (Fig. 5). The actual locations of the measured specimens are given in Table 1.

3.2.1. Skin layer

What is called the 'skin layer' was described in the previous section. It solidifies when the polymer, that had been subject to an elongational flow due to fountain flow, enters into contact with the mold [4]. As the polymer is cooled at a very high cooling rate [13], a lower crystallinity can be expected in this layer: about 5–10% less than in the rest of the plate thickness (Fig. 8). The variation in the crystallinity within the depth explains the lower diffracted crystalline intensity in the skin (Figs. 9(a) and 10(a)) and to a lesser degree the diffracted intensity variations in the others layers (Figs. 9(a)–(d) and 10(a)–(d)).

Lovinger [30] showed that when PP films were crystallized with a high temperature gradient, the lamellae grow in the direction of the temperature gradient. For our skin layer specimen, the orientation function of the *a*-axis relative to the normal direction is low and even negative ($f_{a\mathrm{N}} = -0.03$, Table 1). The *a*-axis is rather oriented in the transverse direction. The effect of the thermal gradient cannot be observed in our specimen. This observation agrees with some recent papers [31,32].

The orientation of the skin layer does not seem very large: the calculated orientation function of the crystalline axis is lower than 0.05. Nevertheless, the skin pole figure (Fig. 10(a)) reveals a maximum of the (040) planes 40° tilted towards the core from the flow direction. This maximum induces a logical maximum of (110) planes in the transverse direction (Fig. 9(a)). From this observation, it is possible to rebuild the crystallite orientation: crystal growth (*a*-axis) in the transverse direction and the *c*-axis tilted 40° towards the core. Therefore, the orientation function of *c*-axis calculated in the local symmetry reference axis would be nearly four times higher than the one calculated in the flow direction or in the normal direction ($f_{c\mathrm{F}} = 0.02 - f_{c\mathrm{N}} = 0.05$): this explains the low orientation values obtained in infrared dichroism. This result was also found for the skin layer of an

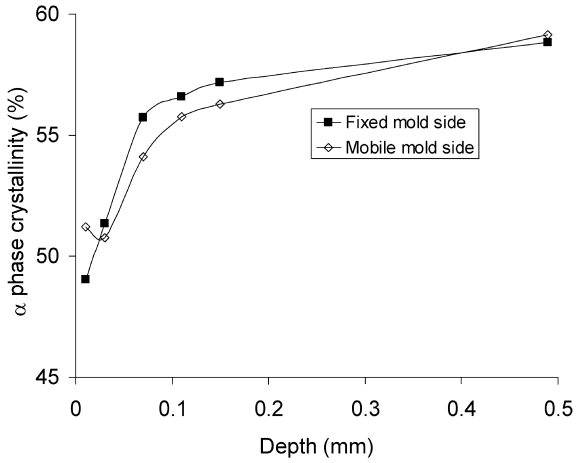

Fig. 8. α phase crystallinity within the depth of a 1 mm-thick injection molded iPP plate, determined by means of a gradient density column. Density of the amorphous phase = 854 kg/m^3, density of α-crystalline phase = 954 kg/m^3, mold temperature = 40 °C, injection time = 1.6 s, zone A, plate 1.

Table 1
Molecular orientation functions from IR dichroism and WAXS measurements. Mold temperature = 40 °C, injection time = 1.6 s, zone A, plate 2

Thickness (mm)	Distance from surface (mm)	Layer	IRD	WAXD								
			f_{cr}	f_{aF}	f_{aT}	f_{aN}	f_{bF}	f_{bT}	f_{bN}	f_{cF}	f_{cT}	f_{cN}
1	0.175	Shearing	0.51	−0.07	0.14	−0.06	−0.41	0.19	0.22	0.47	−0.32	−0.15
	0.350	Post-filling	0.34	−0.07	0.07	−0.01	−0.31	0.19	0.13	0.37	−0.26	−0.12
	0.525	Core	0.04	−0.03	0.07	−0.04	0.01	−0.04	0.03	0.03	−0.04	0.02
3	0.035	Skin	0.04	−0.01	0.04	−0.03	−0.01	0.03	−0.02	0.02	−0.07	0.05
	0.175	Shearing	0.28	0.03	0.02	−0.05	−0.28	0.17	0.11	0.24	−0.18	−0.06
	0.630	Post-filling	0.15	0.02	0.03	−0.05	−0.15	0.10	0.05	0.13	−0.13	0.01
	1.470	Core	−0.01	−0.03	0.05	−0.02	0.00	0.01	−0.02	0.03	−0.07	0.04

injection molded iPP with low injection speed by Kadota et al. [31], but it is still difficult to explain precisely the local structure formation and the tilt angle of the local symmetry directions in this layer where extensional flow due to fountain flow coincides with a very high thermal gradient. Moreover, is the local deformation really known in this layer, since the crystallization kinetics cannot be assessed at such a cooling rate?

3.2.2. Shearing layer

The (110) pole figures of the shearing layer exhibit two maximums (Figs. 9(b) and 11(a)).

- One in the pole figure center, which exhibits a significant

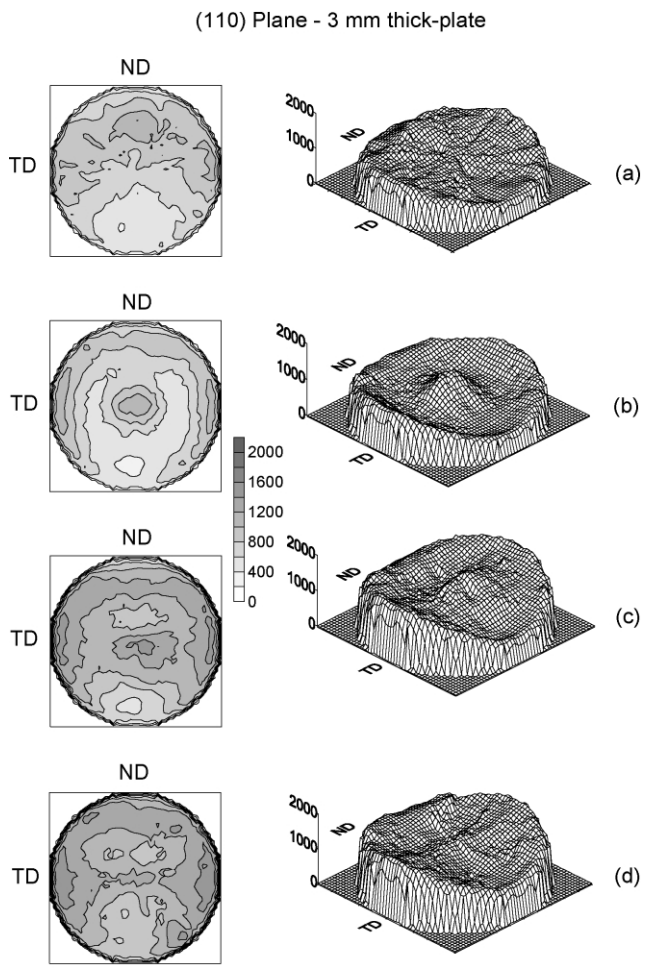

Fig. 9. Contour plots and surface plots of pole figures (110 plane of α-crystalline phase) in the ND–TD plane at different locations within the depth of a 3 mm-thick injection molded iPP plate: (a) skin layer, (b) sheared layer, (c) post-filling layer, and (d) core layer.

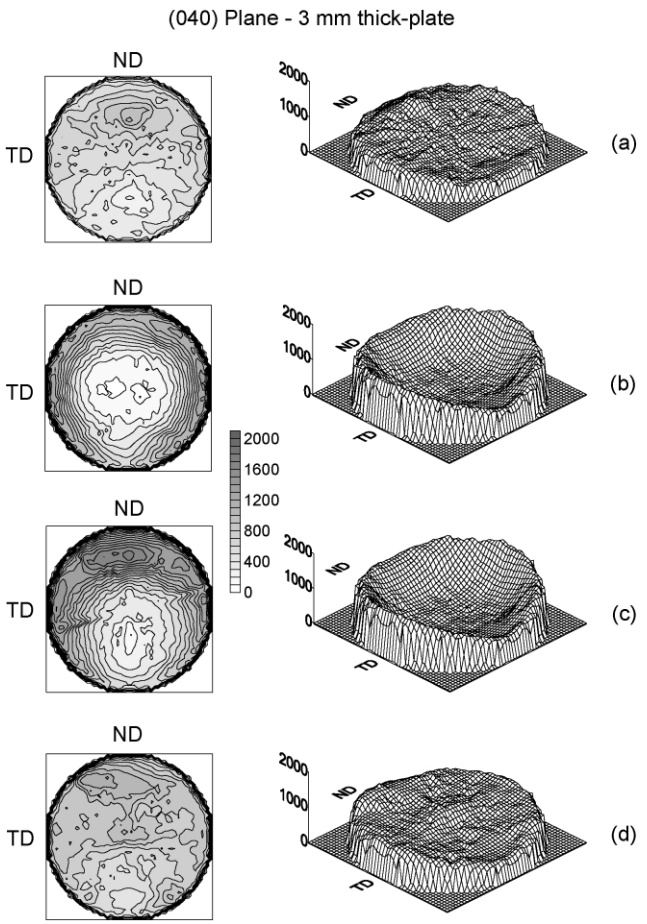

Fig. 10. Contour plots and surface plots of pole figures (040 plane of α-crystalline phase) in the ND–TD plane at different locations within the depth of a 3 mm-thick injection molded iPP plate: (a) skin layer, (b) sheared layer, (c) post-filling layer, and (d) core layer.

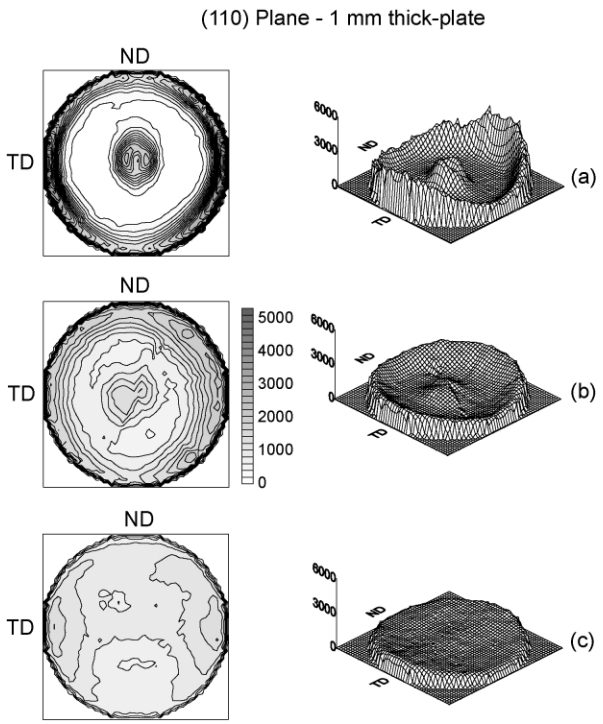

Fig. 11. Contour plots and surface plots of pole figures (110 plane of α-crystalline phase) in the ND–TD plane at different locations within the depth of a 1 mm-thick injection molded iPP plate: (a) sheared layer, (b) post-filling layer, and (c) core layer.

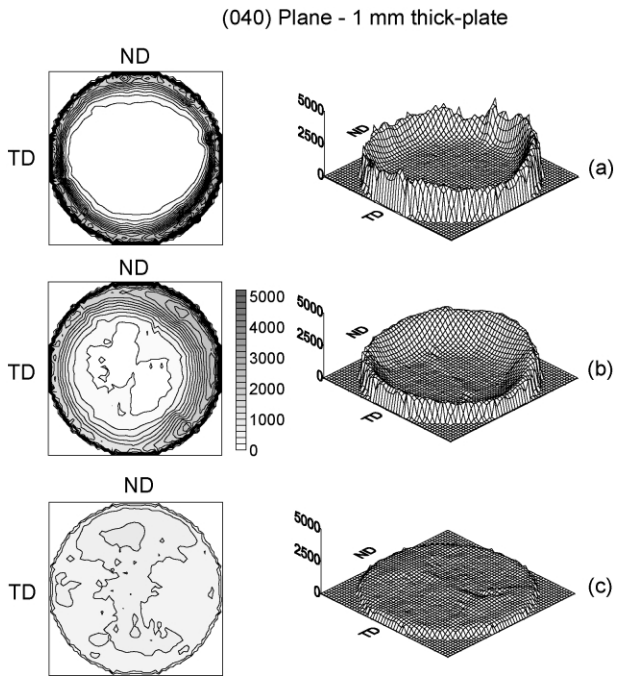

Fig. 12. Contour plots and surface plots of pole figures (040 plane of α-crystalline phase) in the ND–TD plane at different locations within the depth of a 1 mm-thick iPP plate: (a) sheared layer, (b) post-filling layer, and (c) core layer.

amount of (110) planes have its normal oriented in the flow direction, typical of an a^*-axis orientation in the flow direction.

- Another higher maximum around the circumference of the pole figure. Therefore, another fraction of (110) planes has its normal perpendicular to the flow direction that corresponds to a c-axis orientation in the flow direction.

This bimodal orientation has been seen in iPP samples submitted to extensional or shear flows [33].

The crystalline structure is not uniaxial. The diffractograms exhibit a higher diffracted intensity of (110) plane in the transverse direction compared to the normal direction for both the a^*-axis and the c-axis orientations, especially for the 1 mm-thick plate. According to the (040) pole figures (Figs. 10(b) and 12(a)), the main lamellae orientation can be rebuilt (Fig. 13). A large amount of the c-axis oriented lamellaes have their chain axes parallel to the flow direction and they grow in the transverse direction. The most part of the a^*-axis oriented lamellaes have their c-axis oriented in the normal direction. Nevertheless, the a^*-axis orientation of the lamellaes around the flow direction is less pronounced than the c-axis orientation. This crystalline structural model is verified for the shearing layer of 1 and 3 mm-thick samples, and confirmed by the calculated orientation functions (Table 1). As a consequence, nearly no b-axis orientation can be found in the flow direction.

Fujiyama and Wakino [33] propose estimating the respective quantity of the a^*-axis oriented component and the c-axis oriented component by determining the respective areas under the two maximums of (110) plane intensity in an azimuthal scan in the FD–TD plane. According to the same principle, as pole figures were determined in our specimen, we propose to calculate the volumes under each maximum of the (110) pole figures according to Eqs. (8) and (9). To do the calculation, the isotropic intensity level of the crystalline

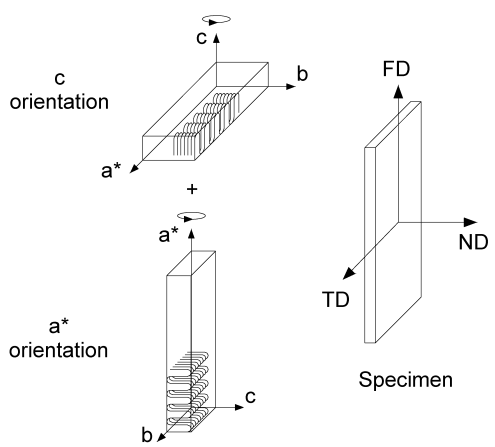

Fig. 13. Main spatial distribution of the crystalline lamellaes in the sheared layers of injection molded iPP plates.

phase was first determined (I_{isotr}) :

$$R_{a^*} = \frac{\int_0^{2\pi}\int_0^{\pi/4}(I(\phi,\beta) - I_{isotr.})\sin\phi\,d\phi\,d\beta}{\int_0^{2\pi}\int_0^{\pi/2} I_{isotr.}\sin\phi\,d\phi\,d\beta} \quad (8)$$

$$R_c = \frac{\int_0^{2\pi}\int_{\pi/4}^{\pi/2}(I(\phi,\beta) - I_{isotr.})\sin\phi\,d\phi\,d\beta}{\int_0^{2\pi}\int_0^{\pi/2} I_{isotr.}\sin\phi\,d\phi\,d\beta} \quad (9)$$

where R_{a^*} and R_c are, respectively, the ratio of the a^*-axis oriented component and the ratio of the c-axis oriented component, the results are recapitulated in Table 2. As the level of the c-axis oriented component increases, that of the a-axis does also. But it seems that the high cooling rates in the 1 mm-thick plates limit the secondary crystallization a^* (Table 2).

Several authors [34,35] attribute the formation of this bimodal orientation to the formation of a secondary crystalline daughter lamellae, which grows epitaxially between the parent lamellae of the row structure. Parent and daughter lamellae should have a parallel b-axis to ensure better nucleation of the secondary crystallization. Apparently, our crystalline structural model does not agree with the fact that the b-axis of a^*-axis (daughter) and c-axis (parent) oriented lamellaes are parallel if one only looks at the main lamellae orientations (Fig. 13). But knowing that the a^*-axis component is lower in amount than the c-axis component (Table 2) and that the two components have a large orientation distribution, the a^*-axis lamellae could nucleate locally on the c^*-axis lamellae, which have the same crystallographic b-axis. Therefore, our crystalline structural model would not contradict the previous authors.

Although the same crystalline structure is found in the 1 and 3 mm-thick samples, a large difference of orientation level can be seen in Fig. 14. The shearing layer of the 1 mm-thick sample exhibit almost a fully bimodal orientation. More than the injection speed, the influence of thickness, that is the cooling rate, influences the crystalline orientation generated by the shear-induced crystallization. Orientation measurements by WAXS confirm the previous results obtained by infrared dichroism measurements (Fig. 7).

3.2.3. Post-filling layer

Pole figures of post-filling layers have the same shape as those of the shearing layers, but with attenuated intensity variations and a significantly higher level of isotropic crystalline polymer. The values of orientation functions (Table 2) are lower, but they vary in the same way. Therefore, a^* and c-axis oriented components contribute to give qualitatively the same crystalline structural model, which is described in Fig. 13.

As the local axes of symmetry of the 1 mm-thick specimen merge with the flow, transverse and normal directions, those of the 3 mm-thick specimen are tilted by about 30° towards the core. The tilt angle of the local axes of symmetry in the post-filling zone has been observed by several researchers including Mavridis et al. [36] and more recently Kadota et al. [31], but the formation mechanism of this crystalline structure is difficult to explain.

During the post-filling, the shear rate is very low (typically less than 1 s^{-1}) and the shear-induced crystallization should not lead to high levels of molecular orientation. Wang and Cakmak [37] suggested that the crystalline structure is the result of the mix of 'apparently' unoriented spherulitic structure and high extended crystallites (treads) formed upstream, which were transported downstream by the surrounding melt polymer. This hypothesis is not unreasonable, but the polarized optical micrographs do not indicate the presence of highly birefringent crystalline treads. We believe rather that oriented nuclei are formed during the filling and post-filling stages while the temperature approaches the crystallization temperature. These nuclei could be reoriented by the post-filling flow and could generate an oriented crystallization.

This type of phenomenon can be observed in a shearing device [38]: the polypropylene is sheared for few seconds (typically 5 or 10 s at 140 °C) and a shear-induced crystallization can be observed several minutes later (1–3 min for the previous shearing conditions), while in fact the melt orientation due to the initial shearing has largely had the time to relax. Then, a significant crystalline orientation can be measured.

3.2.4. Core layer

The level of molecular orientation is small in the core layer. Nevertheless, a small amount of the a^*-axis orientation component seems to remain in the 3 mm-thick sample. Oriented nuclei could have been transported towards the core during the filling and post-filling stages.

Table 2
Assessment of a^* and c oriented components distribution with respect to the flow direction. Mold temperature = 40 °C, injection time = 1.6 s, zone A, plate 2

Thickness (mm)	Layer	a^* oriented ratio (%)	c oriented ratio (%)	Isotropic distribution ratio (%)	a^*/c
1	Shearing	27	65	8	0.41
	Post-filling	9	36	55	0.27
	Core	1	11	88	0.10
3	Shearing	13	18	69	0.68
	Post-filling	9	11	80	0.82
	Core	4	14	82	0.27

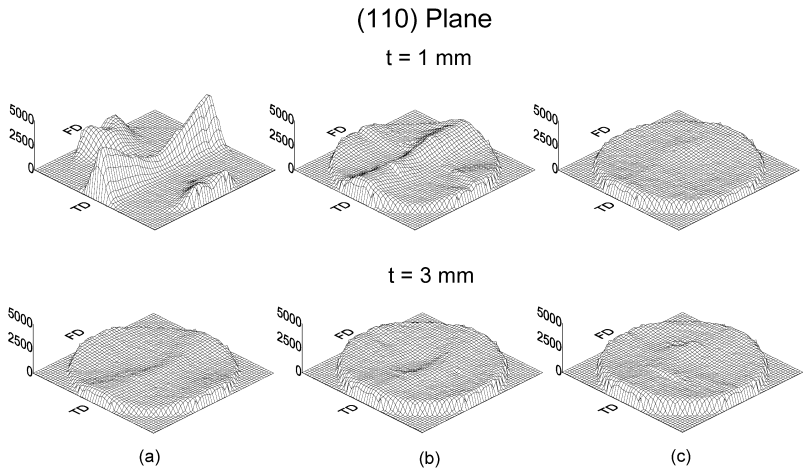

Fig. 14. Comparison of surface plots of pole figures (110 plane of α-crystalline phase) in the FD–TD plane at different locations within the depth of a 1 mm and a 3 mm-thick injection molded iPP plates: (a) sheared layer, (b) post-filling layer, and (c) core layer.

4. Conclusion

Although high levels of chain orientation in the crystal phase can be obtained in injection molded iPP, the orientation of the amorphous phase remains very low. Therefore, the anisotropy of injection molded semi-crystalline polymers is governed by the orientation of the crystalline phase.

The shearing layer exhibits the highest level of crystalline orientation. Despite having almost the same shear layer thickness, the chain orientation in the 1 mm-thick plate is twice as high as that in the 3 mm-thick plate. More surprising is the very low influence of injection speed on the maximum of the chain orientation when it is tripled. Therefore, we can conclude that the thickness of the part is the parameter which governs the global level of crystalline orientation. In other words, the cooling rate is the most influential parameter on the crystalline orientation generated by the flow induced crystallization in the injection molding of iPP.

High levels of chain orientation were found in the skin layer, but the direction of orientation tilted towards the core. This tilting of the local axes of symmetry explains the small orientation function value, which was determined by infrared dichroism. At the moment, it is difficult to describe precisely the mechanism that tilted the orientation induced by the extensional flow at the melt front.

A bimodal crystalline orientation was generated in the shearing flow direction: the chains of the main lamellae ('*c*-axis direction') are oriented in the flow direction while the lamellae principally grow in the transverse direction. The secondary lamellae grow orthogonally to the main lamellae in the flow direction, while their chains are principally parallel to the normal direction. The *b*-axis of the main groups of a^* and *c*-axis oriented lamellaes do not have the same direction, as observed by most researchers, but this result does not contradict the literature because this property could be locally verified, as the proportion of the a^*-axis oriented component is lower than that of the *c*-axis.

In the post-filling layer, the orientation remains high despite the low shear stresses. Moreover, the bimodal crystalline orientation continues to exist while its local axes of symmetry tilt towards the core. The formation of this crystalline structure could be explained by orientated nuclei which were created during the injection phase and which would rotate under the very slow flow during the post-filling, but is still difficult to clearly explain the tilt of the superstructure local axis. Some of these nuclei could also be transported to the core layer since a small amount of the a^*-axis orientated component seems to remain in the 3 mm-thick sample. Nevertheless the orientation in the core layer is very low.

Acknowledgements

The authors wish to express their gratitude to the companies LEGRAND, MOLDFLOW and SOLVAY for their generous financial support. We also wish to thank H. Algave, D. Delaunay, R. Fulchiron, P. Kennedy, E. Koscher, M. Laplanche, V. Leo, G. Poutot, J.M. Rossignol, and R. Zheng for the useful discussions and help during all of the shrinkage crystallinity orientation of polymers (SCOOP) study.

References

[1] Jansen KMB, Van Dijk DJ, Husselman MH. Polym Engng Sci 1998; 38(5):838.
[2] Phillips R, Herbert G, News J, Wolkowics M. Polym Engng Sci 1994; 34(23):1731.
[3] Ben Dali H, Cole KC, Sanschagrin B, Nguyen KT. J Inject Mold Technol 1998;2(2):59.
[4] Tadmor Z. J Appl Polym Sci 1974;18:1753.
[5] Isayev AI. Polym Engng Sci 1983;23(5):271.

[6] Kamal MR, Tan V. Polym Engng Sci 1979;19:558.
[7] Flaman AAM. Polym Engng Sci 1993;33:193.
[8] Jansen KMB, van Dijk DJ, Burgers EV. Int Polym Process 1998; XIII(3):309.
[9] Pople JA, Mitchel GR, Sutton SJ, Vaughan AS, Chai CK. Polymer 1999;40:2769.
[10] Trotignon JP, Verdu J. J Appl Polym Sci 1987;34:1.
[11] Trotignon JP, Verdu J. J Appl Polym Sci 1990;39:1215.
[12] Fujiyama M, Wakino T. J Appl Polym Sci 1991;42:2739.
[13] Delaunay D, Le Bot P, Fulchiron R, Luye JF, Regnier G. Polym Engng Sci 2000;40(7):1682.
[14] Costa L, Jacobson K, Brunella V, Bracco P. Polym Test 2001;20(6): 649.
[15] Jansen KMB, Orij JJW, Meijer CZ, Van Dick DJ. Polym Engng Sci 1999;39(10):2030.
[16] Lundberg L, Sjönell Y, Stenberg B, Terselius B, Jansson JF. Polym Test 1994;13:441.
[17] Ülçer Y, Camak M. Polymer 1997;38(12):2907.
[18] Jasse B, Koening JL. J Macromol Sci—Rev Macromol Chem 1979; C17(1):61.
[19] Fina LJ, Koening J. J Polym Sci, Part B: Polym Phys 1986;24:2509.
[20] Cole KC, Ajji A. In: Ward IM, Coates PD, Dumoulin MM, editors. Solid phase processing of polymers. Munich/Cincinnati: Hanser/ Hanser Gardner; 2000. p. 33–84.
[21] Sjönell Y, Terselius B, Jansson JF. Polym Engng Sci 1995;35(11): 950.
[22] Lafranche E, Pabiot J. J Appl Polym Sci 1998;68:1661.
[23] Samuels RJ. Makromol Chem 1981;(Suppl. 4):241.
[24] Samuels RJ. Polym Engng Sci 1988;28(13):852.
[25] Alexander L. X-ray diffraction methods in polymer science. New York: Wiley; 1969.
[26] Karacan I, Taraiya AK, Bower DI, Ward IM. Polymer 1993;34(13): 2691.
[27] Wilchinsky ZW. J Appl Polym Sci 1963;7:923.
[28] Turner J, Aizlewood JM, Becket DR. Eingegangen 1963;8:134.
[29] Bushko WC, Stokes VK. Polym Engng Sci 1995;35(4):365.
[30] Lovinger AJ. Polym Sci, Polym Phys Ed 1983;21:97.
[31] Kadota M, Cakmak M, Hamada H. Polymer 1999;40:3119.
[32] Wang YD, Cakmak M. Polymer 2001;42:4233.
[33] Fujiyama M, Wakino T. J Appl Polym Sci 1991;42:2739.
[34] Clark ES, Spruiell JE. Polym Engng Sci 1976;16:176.
[35] Kumaraswamy G, Verma RK, Issaian AM, Wang P, Kornfield JA, Yeh F, Hsiao BS, Olley RH. Polymer 2000;41:8931.
[36] Mavridis H, Hrymak AN, Vlachopoulos J. Polym Engng Sci 1986; 26(7):449.
[37] Wang YD, Cakmak M. Polymer 2001;42:3731.
[38] Koscher E, Fulchiron R. Polymer 2002;43:6931.